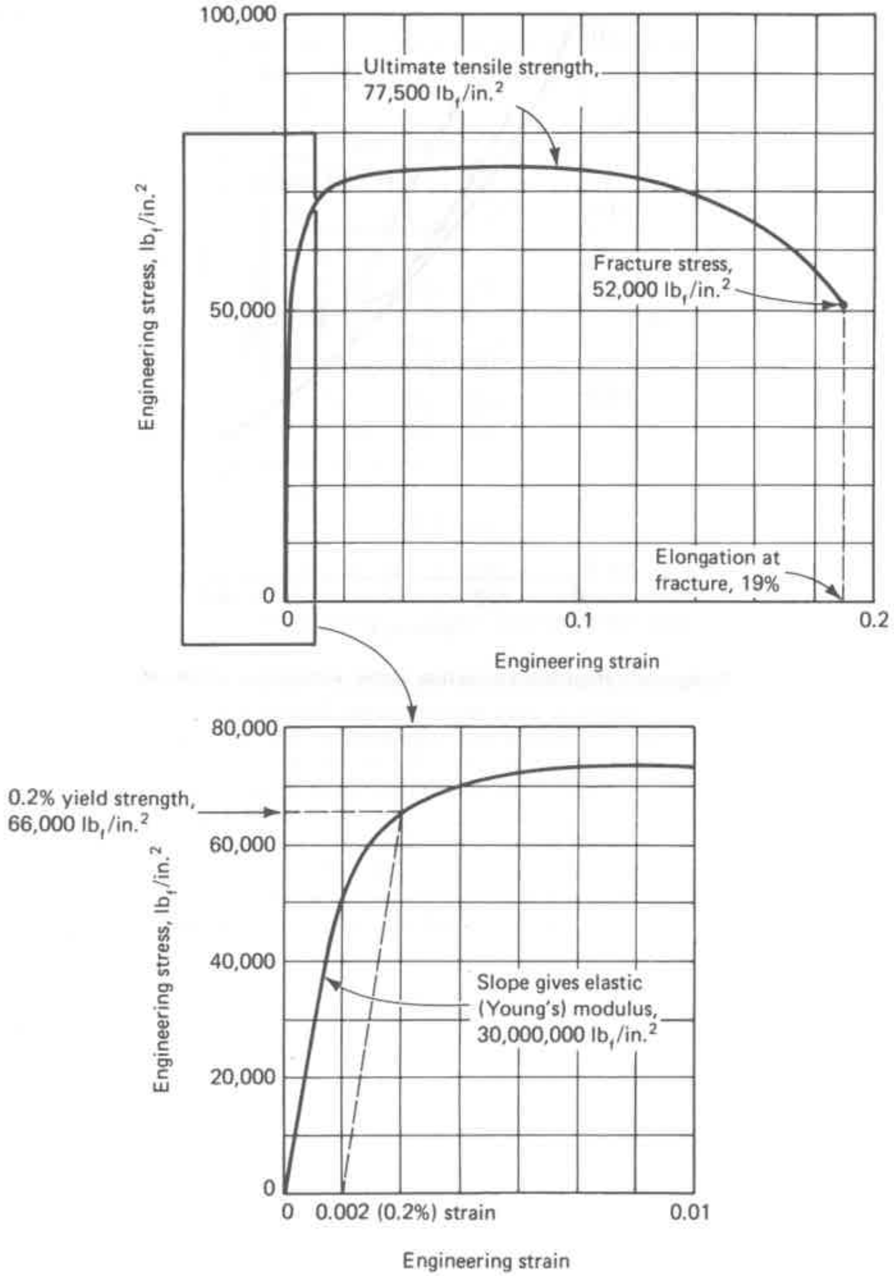

Engineering stress–engineering strain curve of 0.2% C plain carbon, cold worked steel, showing definition of mechanical property terms.

Source: Charlie R. Brooks, Heat Treatment, Structure and Properties of Nonferrous Alloys, American Society for Metals, Metals Park OH, 1982, p 2

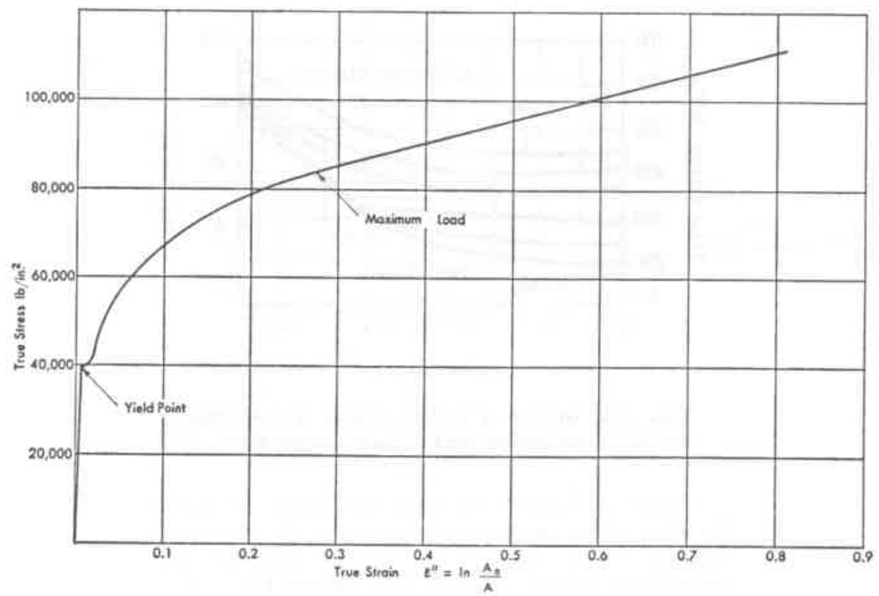

True-stress versus true-strain diagram or physical stress-strain diagram for mild steel.

Source: Donald S. Clark, Engineering Materials and Processes, International Textbook Co., Scranton PA, 1962, p 36

11-21. Type 403 Stainless Steel

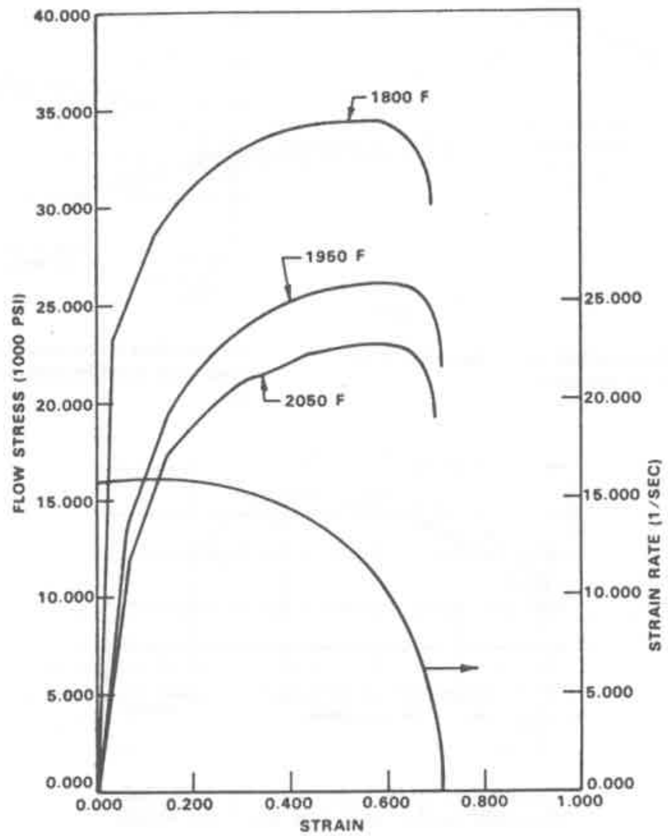

Flow stress versus strain, and strain rate versus strain, for type 403 stainless steel at 1800, 1950, and 2050 °F (tests were conducted in a mechanical press where $\dot{\epsilon}$ was not constant).

Source: Metal Forming, Taylan Altan, Soo-Ik Oh and Harold L. Gegel, Eds., American Society for Metals, Metals Park OH, 1983, p 52

11-22. Type 410 Stainless Steel

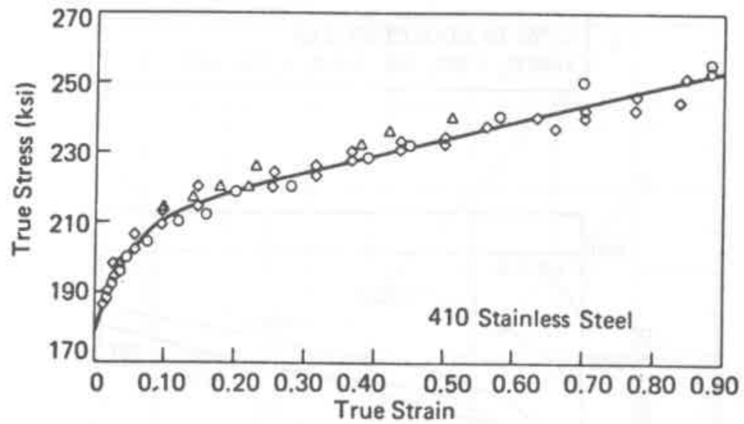

Room-temperature tensile and compressive flow curves.

Source: R. Chait, Factors Influencing the Strength Differential of High Strength Steels, Met. Trans. A, February 1972, American Society for Metals, Metals Park OH, p 367

12-12. Inconel Alloy 625

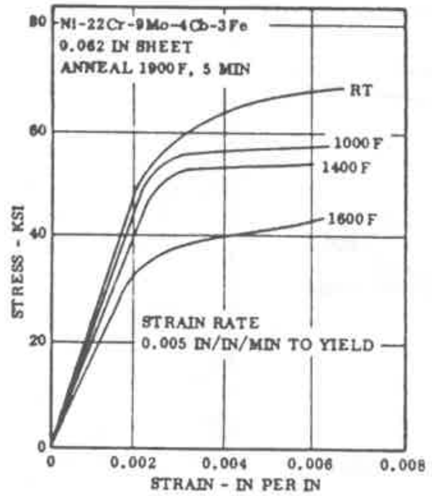

Stress-strain curves for 0.062-in. sheet at room and elevated temperatures.

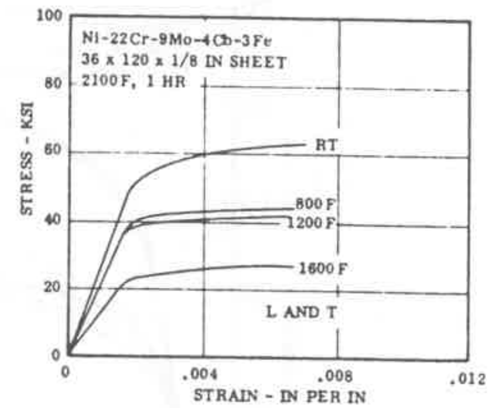

Stress-strain curves in tension for 1/8-in. sheet at room and elevated temperatures.

Source: Aerospace Structural Metals Handbook, Volume 4, Mechanical Properties Data Center, Battelle Columbus Laboratories, Columbus OH, 1981, p 12

12-13. Inconel Alloy 702

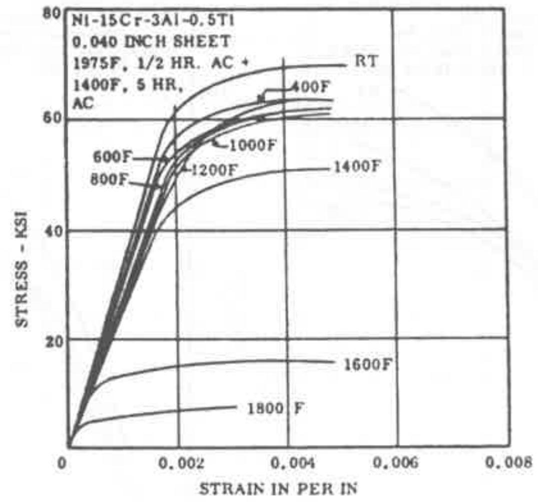

Temperature stress-strain curves at various temperatures.

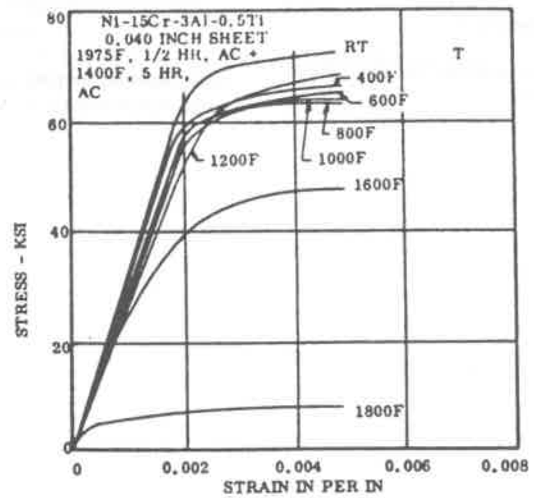

Compressive stress-strain curves at temperature.

Source: Aerospace Structural Metals Handbook, Volume 4, Mechanical Properties Data Center, Battelle Columbus Laboratories, Columbus OH, 1981, p 3

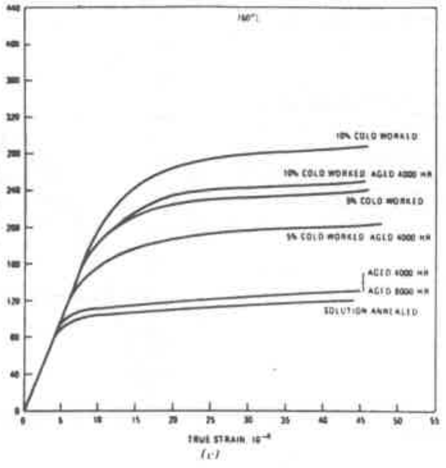

The true stress-strain curves that were measured in this work are displayed in the graphs on this and the previous page. Each curve in these graphs is an average obtained from several tests and represents the general level of the stress-strain curve, ignoring any effects due to serrated yielding. The 0.2% offset yield strengths that were measured from these curves are given in the table below. Here the data are separated, according to specimen treatment, into three categories: solution annealed and cold worked, aged, and cold worked and aged.

Summary of 0.2 Pct Offset Yield Strengths (in MPa) Measured in This Work

	Aging and Testing Temperature, °C				
Specimen	538	593	649	704	760
Solution annealed	131	124	124	124	110
5 pct c.w.	276	248	234	220	227
10 pct c.w.	331	303	310	296	276
Aged 4000 h	214	282	220††	145††	124
Aged 8000 h	227	–	276†	–	124
5 pct c.w.; aged 4000 h	317	393††	262†	207	193
	(358)	(407)	(331)	(241)	(241)
10 pct c.w.; aged 4000 h	420	462	324†	276†	234
	(413)	(462)	(407)	(317)	(289)

Note: The entries marked with a dagger correspond to specimens which showed γ' formation in the matrix, while the entries marked with a double dagger showed γ' formation in the grain boundaries. The entries enclosed in parentheses correspond to the yield strengths predicted by the Hall-Petch relation.

Source: R. E. Villagrana, J. L. Kaae, J. R. Ellis and P. K. Gantzel, The Effect of Aging and Cold Working on the High-Temperature Low-Cycle Fatigue Behavior of Alloy 800H: Part I—The Effect of Hardening Processes on the Initial Stress-Strain Curve, Met. Trans. A, July 1978, American Society for Metals, Metals Park OH, p 932–933

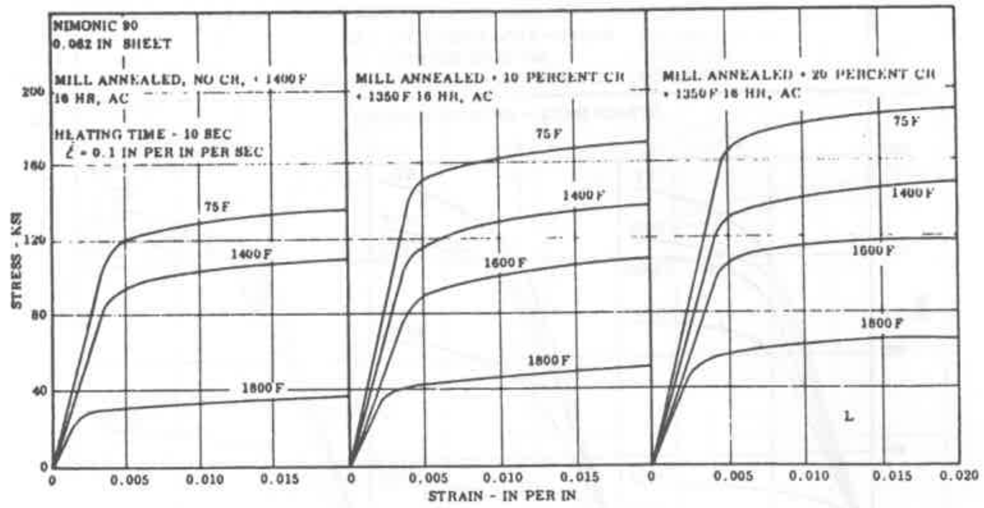

Stress-strain curves determined at various temperatures at a rapid strain rate after rapid heating of sheet cold rolled 0, 10, and 20 percent between mill annealing and aging.

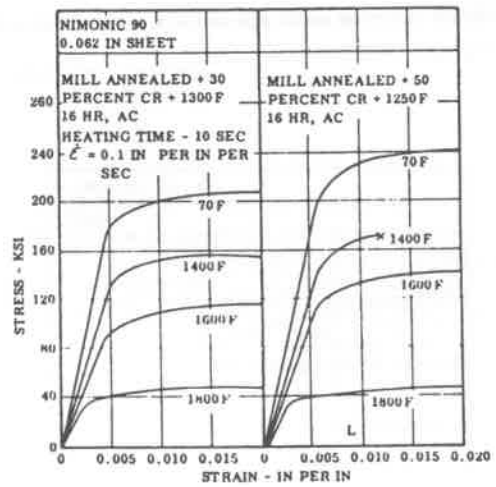

Stress-strain curves determined at various temperatures at a rapid strain rate after rapid heating of sheet cold rolled 30 and 50 percent between mill annealing and aging.

Source: Aerospace Structural Metals Handbook, Volume 5, Mechanical Properties Data Center, Battelle Columbus Laboratories, Columbus OH, December 1978, p 7

13-14. Three Grades of Malleable Iron

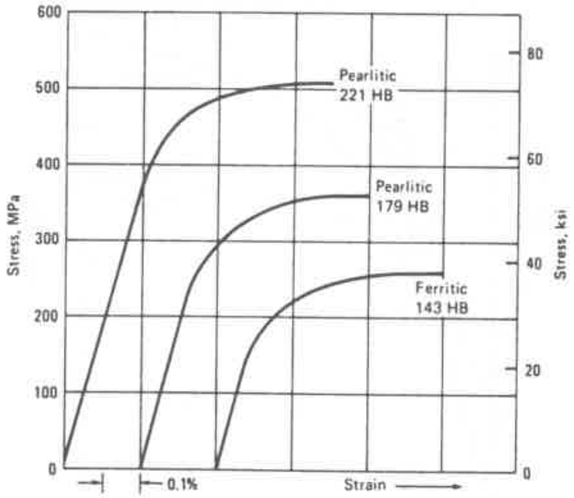

Stress-strain curves for three malleable irons.

Modulus of elasticity in tension is about 170 GPa (25 $\times$ 10^6 psi). The figure above shows typical stress-strain curves for ferritic and pearlitic malleable irons. The modulus in compression ranges from 150 to 170 GPa (22 $\times$ 10^6 to 25 $\times$ 10^6 psi); in torsion, from 65 to 75 GPa (9.5 $\times$ 10^6 to 11 $\times$ 10^6 psi).

Source: Metals Handbook, Ninth Edition, Volume 1, Properties and Selection: Irons and Steels, American Society for Metals, Metals Park OH, 1978, p 65

13-15. Pealitic and Ferritic Malleable Iron

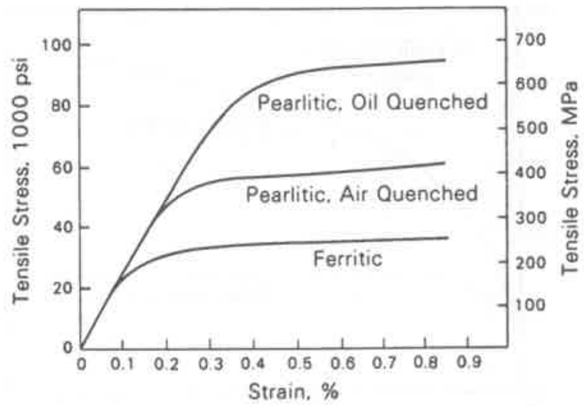

Typical stress-strain curves obtained from machined cast-to-shape test bars for three types of malleable iron.

The typical stress-strain curves for various types of malleable iron shown in the graph above were obtained from machined tensile test bars. The modulus of elasticity generally decreases with an increasing amount of graphite and less compact graphite nodule shape. The matrix structure has little influence except in the case of pearlitic irons in which the amount of graphite is reduced, thereby improving the modulus. Various moduli from 22.8 to 24.6 $\times$ 10^6 psi (157.2 to 169.6 GPa) are reported for ferritic irons and 22.4 to 25.8 $\times$ 10^6 psi (154.4 to 177.9 GPa) for various pearlitic irons. The modulus of elasticity may also be accurately measured dynamically in an Elastomat or in bending.

Source: Iron Castings Handbook, Charles F. Walton, Ed., Iron Castings Society, Inc., 1981, p 304

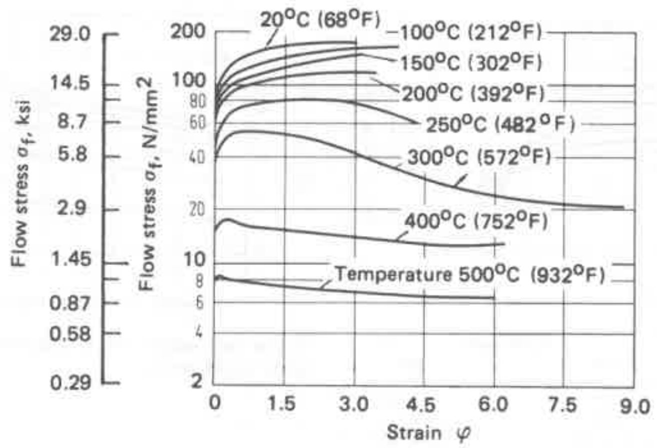

Flow stress of aluminum (technical purity) as a function of strain at different temperatures.

The flow curves in the figure above exhibit a maximum stress at about 220 °C (428 °F). Their shapes can be explained qualitatively by the "climbing" of dislocations, which takes place at elevated temperatures.

Since both recovery and recrystallization take place at a finite temperature-dependent rate, flow stress depends strongly on the strain rate. At a given temperature the effect of the strain rate on flow stress can be approximated by the relation

$$\sigma_f = \sigma_{f,1}\left(\frac{\dot{\varphi}}{\dot{\varphi}_1}\right)^m$$

where $\sigma_{f,1}$ is the flow stress at the strain rate $\dot{\varphi}_1$. For steels typical values of the exponent m range from -0.02 to $+0.05$ at 20–450 °C (68–845 °F) and from 0.1 to 0.2 at temperatures above 880 °C (1616 °F).

Source: Handbook of Metal Forming, Kurt Lange, Ed., McGraw-Hill Book Co., New York, 1985, p 4.4

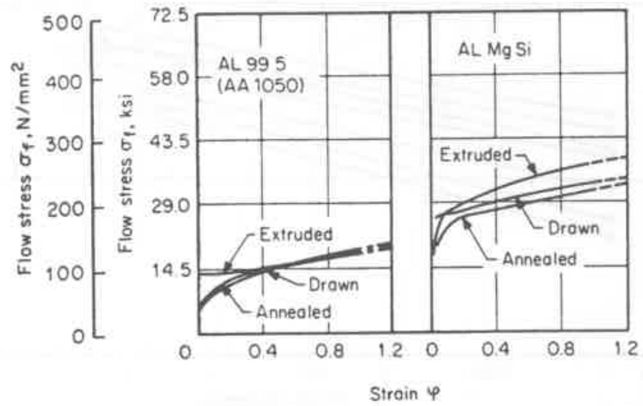

Flow curves of some aluminum alloys.

In the more general case the hardening coefficient cannot be assumed to be constant, that is,

$$n = n(\varphi).$$

Source: Handbook of Metal Forming, Kurt Lange, Ed., McGraw-Hill Book Co., New York, 1985, p 4.13

16-29. Commercial Bronze (C22000)

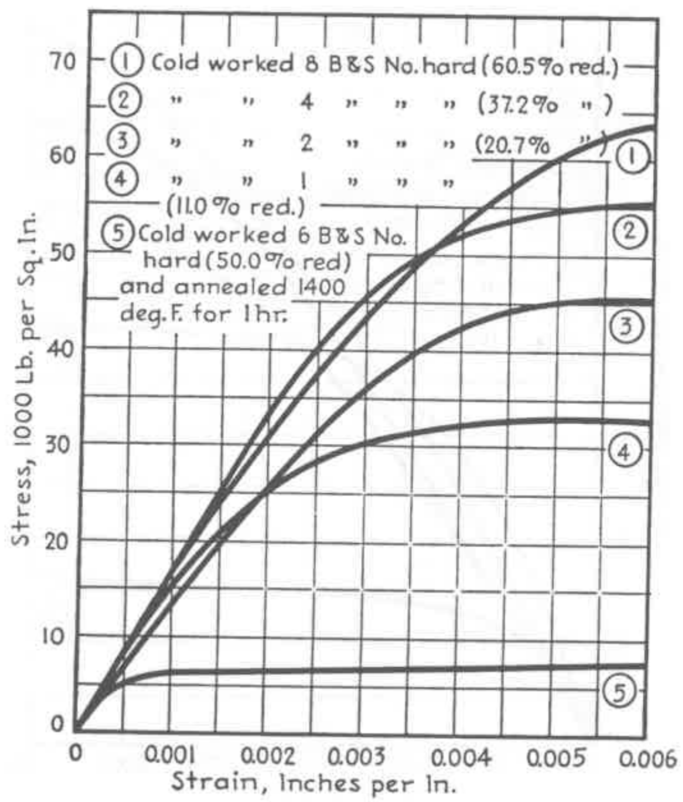

The effect of cold working on the stress-strain characteristics of commercial bronze (Government-gilding) strip (0.040 in. thick) having a ready-to-finish grain size of 0.070 mm. (89.74% copper); 5,000-lb. capacity hydraulic testing machine and Templin automatic extensometer accurate to 0.00001 in. were used.

Source: R. A. Wilkins and E. S. Bunn, Copper and Copper Base Alloys, McGraw-Hill Book Co., New York, 1943, p 38

16-30. Red Brass (C23000)

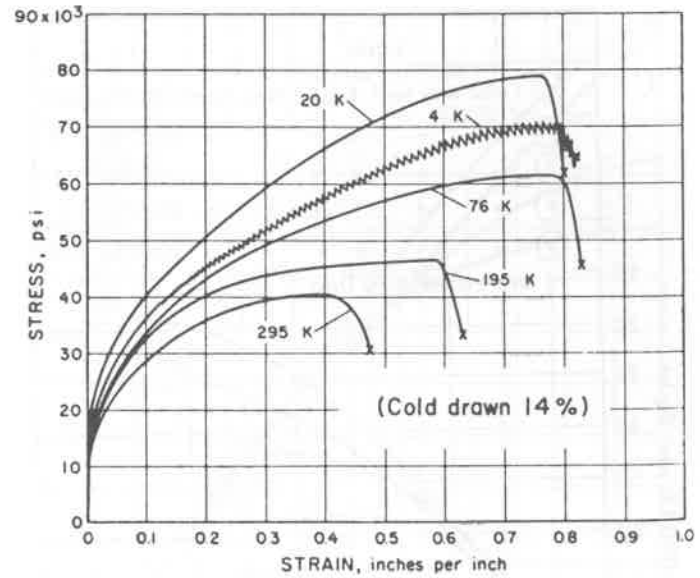

Source: Source Book on Copper and Copper Alloys, American Society for Metals, Metals Park OH, 1979, p 34

16-73. 80-20 Cupro-Nickel (C71000)

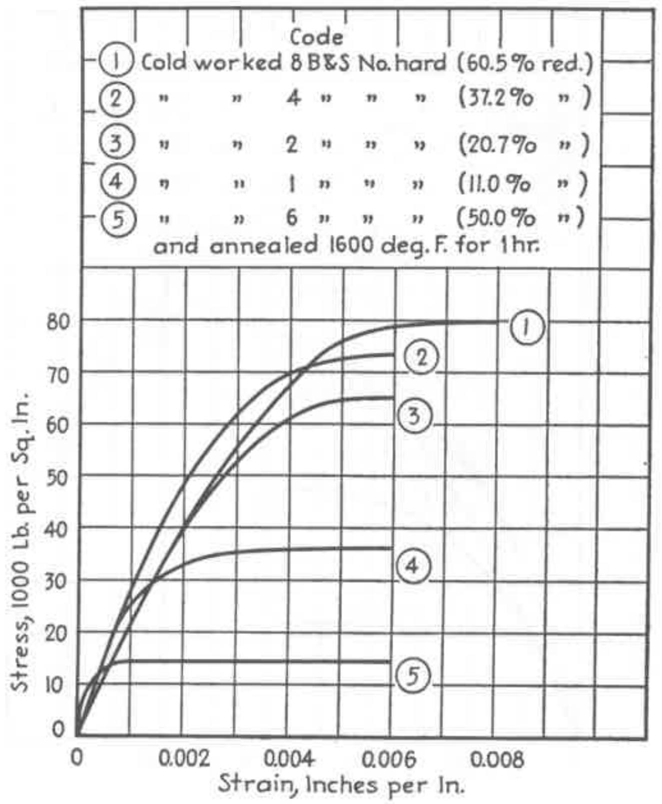

The effect of cold rolling on the stress-strain characteristics of 80-20 cupro-nickel strip (0.040 in. thick) having a ready-to-finish grain size of 0.055 mm.; 5,000-lb. capacity hydraulic testing machine and Templin automatic extensometer accurate to 0.00001 in. were used (79.18% copper, 20.65% nickel, 0.51% manganese).

Source: R. A. Wilkins and E. S. Bunn, Copper and Copper Base Alloys, McGraw-Hill Book Co., New York, 1943, p 237

16-74. 70-30 Cupro-Nickel (C71500)

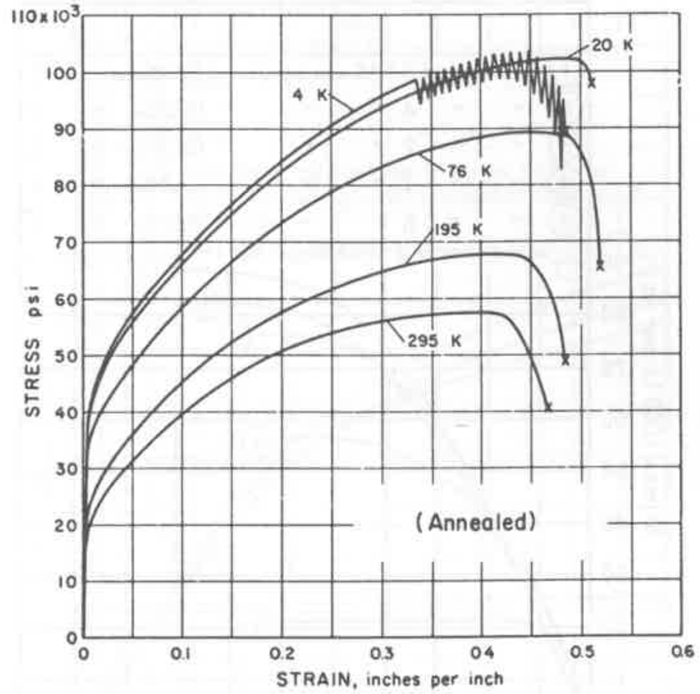

Source: Source Book on Copper and Copper Alloys, American Society for Metals, Metals Park OH, 1979, p 36

16-97. Copper-Nickel-Aluminum Alloy (Sand Cast)

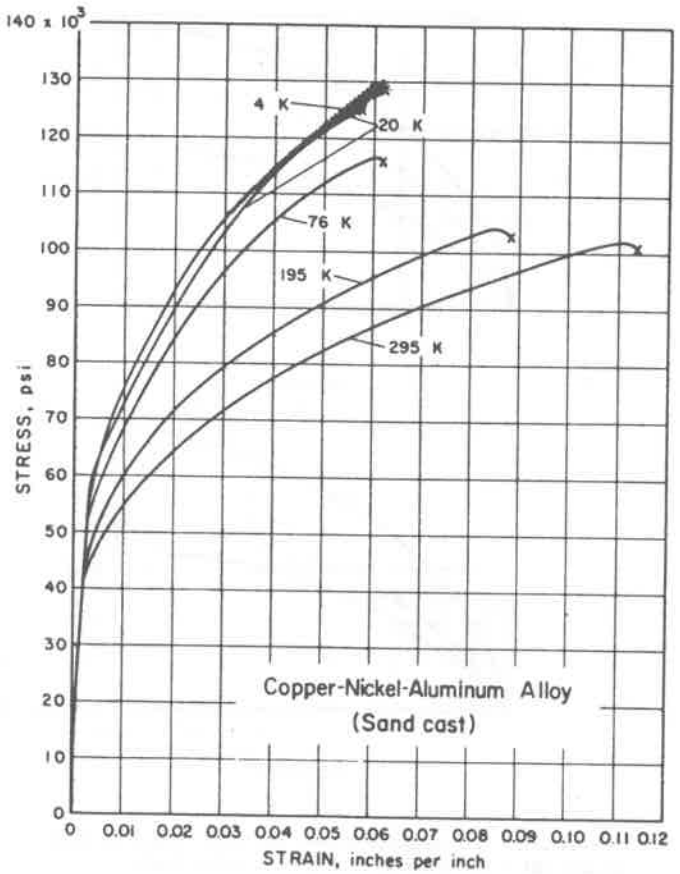

Source: Source Book on Copper and Copper Alloys, American Society for Metals, Metals Park OH, 1979, p 37

16-98. Copper vs Aluminum Alloys

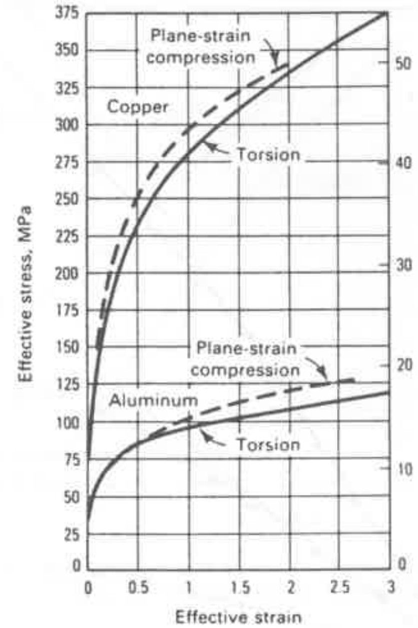

Comparison of room-temperature flow curves from torsion and plane-strain compression tests on copper and aluminum.

Source: Metals Handbook, Ninth Edition, Volume 8, Mechanical Testing, American Society for Metals, Metals Park OH, 1985, p 164

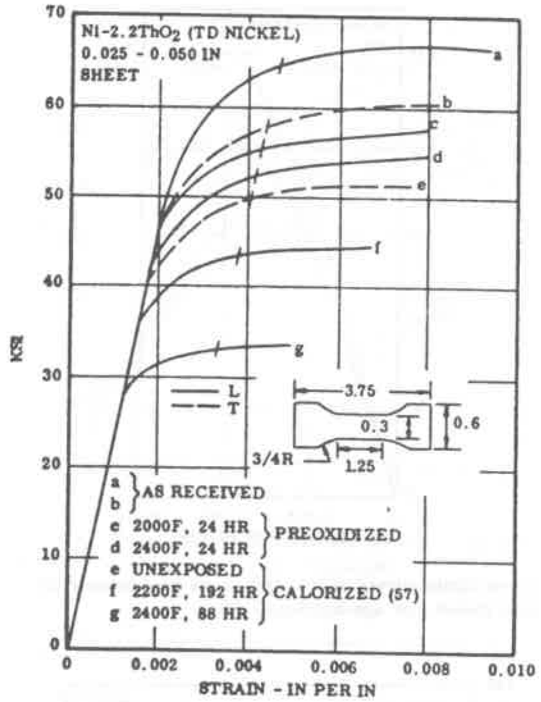

Stress-strain curves at room temperature for sheet.

Source: Aerospace Structural Metals Handbook, Volume 4, Mechanical Properties Data Center, Battelle Columbus Laboratories, Columbus OH, 1981, p 9

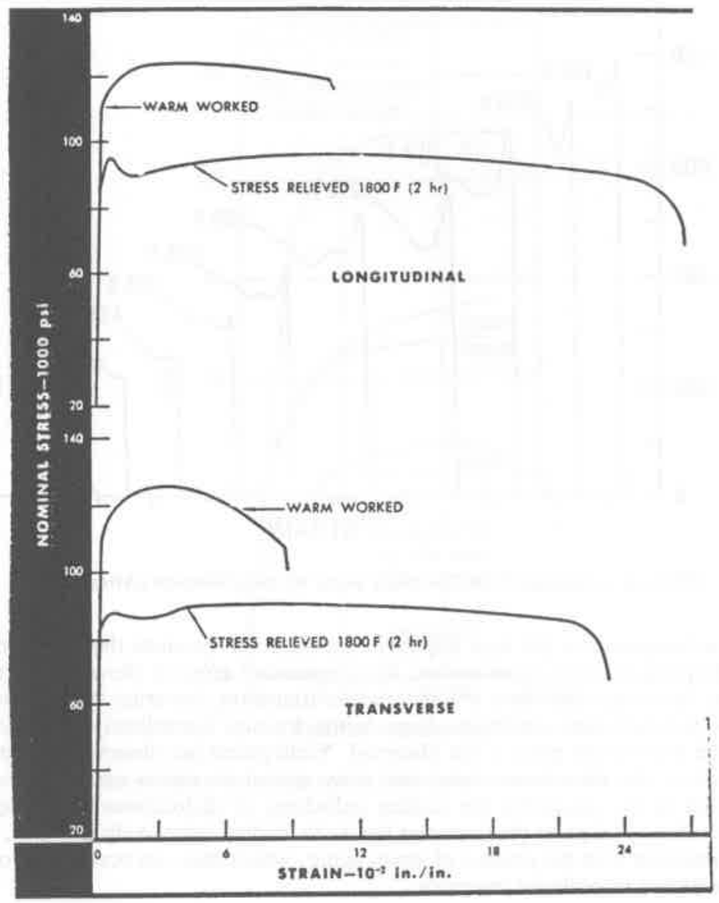

Effect of stress relieving on the stress-strain curves of unalloyed arc-cast molybdenum sheet with nominal thickness of 0.030 to 0.040 in., strain rate 0.025 in./in./min.

Source: Molybdenum Metal, Climax Molybdenum Company, 1960, p 29

23-24. Thorium-Carbon Alloys

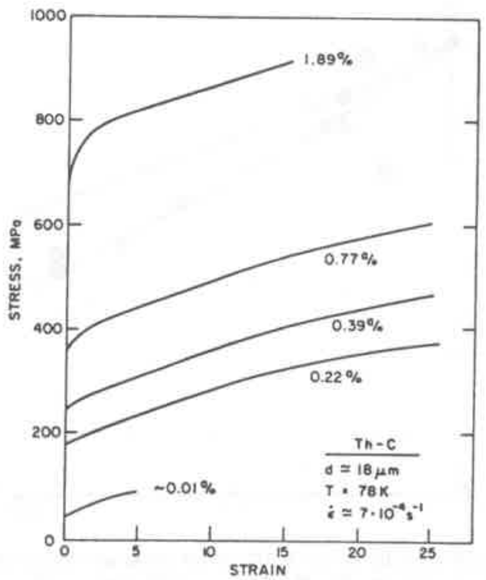

True tensile stress-strain curves for thorium-carbon alloys. (After Peterson and Skaggs.)

Source: Deformation, Processing, and Structure, George Krauss, Ed., papers presented at the ASM Materials Science Seminar, 23 October 1982, St. Louis MO, sponsored by the Seminar Committee of the Materials Science Division of the American Society for Metals, Metals Park OH, 1984, p 95

23-25. Tin and Lead

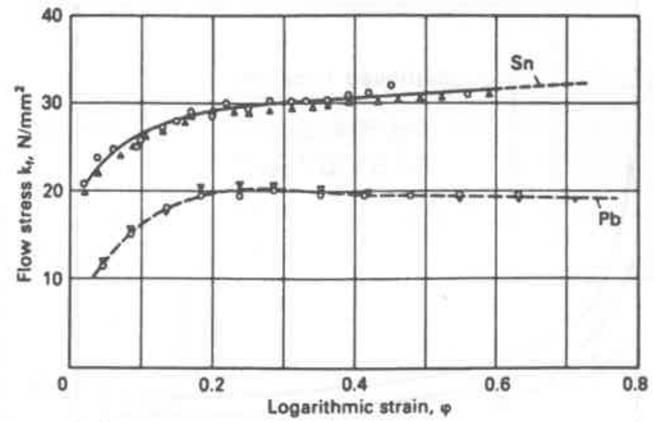

Stress-strain curves of lead and tin at room temperature.

Source: Kurt Laue and Helmut Stenger, Extrusion Processes: Machinery Tooling, trans. A. F. Castle and Gernot Lang, American Society for Metals, Metals Park OH, 1976, p 117

23-26. Unalloyed Uranium

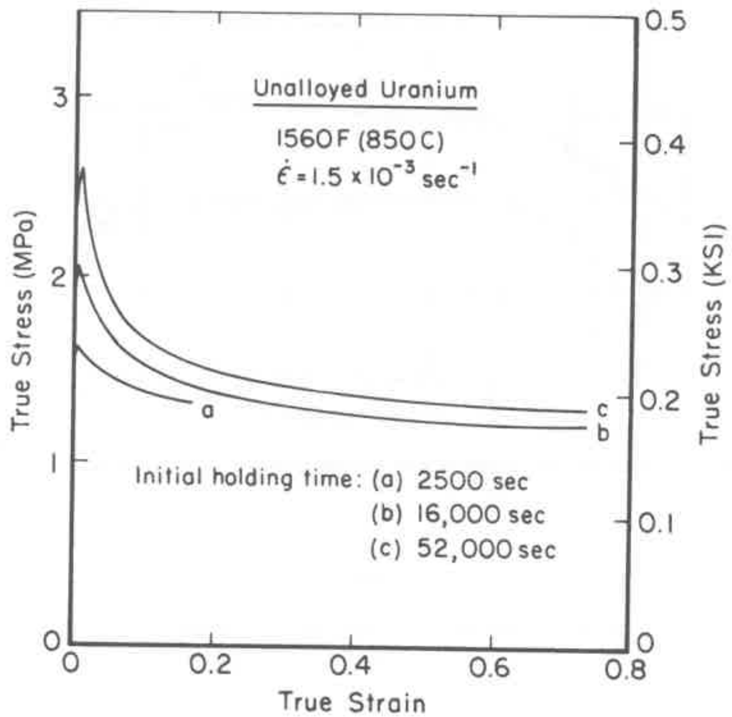

Compression flow curves for unalloyed depleted uranium tested in the gamma phase field that exhibit high levels of flow softening. Test specimens were held at 850 °C (1560 °F) in an atmosphere containing 10 ppm oxygen for the times indicated prior to testing. The external oxide layer formed on holding led to high initial flow stresses but broke up rapidly with strain beyond a few percent deformation.

Perhaps the first reported instance of flow instability under compressive loading is that of Jonas and Luton. While establishing the general sources of flow softening at elevated temperatures, they found unusual, localized bulges in specimens of oxidized uranium isothermally upset at 850 °C (1562 °F) and $\dot{\epsilon} \approx -1.5 \times 10^{-3}\ s^{-1}$. For this material, the stress-strain curves (see above) showed large amounts of flow softening whose magnitude depended on the holding time prior to testing, during which oxide layers of increasing thickness developed on the specimen surface.

Source: S. L. Semiatin and J. J. Jonas, Formability and Workability of Metals, American Society for Metals, Metals Park OH, 1984, p 56

23-27. Lithium-Potassium-Sodium

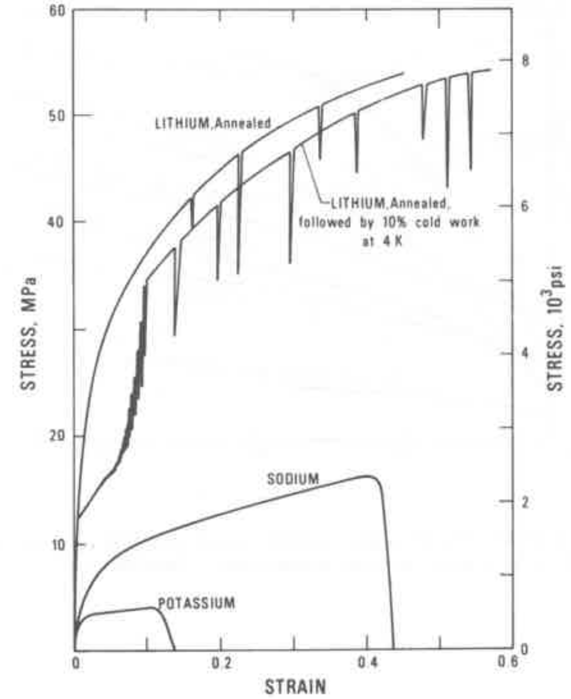

Stress-strain curves at 4 K of annealed polycrystalline sodium, potassium, lithium, and cold-worked lithium (After Reed; Hull and Rosenberg.)

Source: Materials at Low Temperatures, Richard P. Reed and Alan F. Clark, Eds., American Society for Metals, Metals Park OH, 1983, p 315

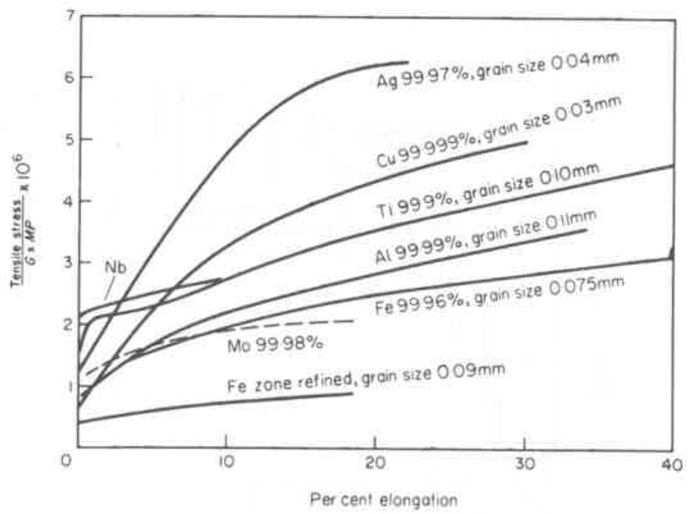

Stress-strain curves of polycrystalline metals compensated for differences in melting point and elastic modulus. (After McLean.)

Source: R. W. K. Honeycombe, The Plastic Deformation of Metals, Second Edition, American Society for Metals, Metals Park OH, 1984, p 239

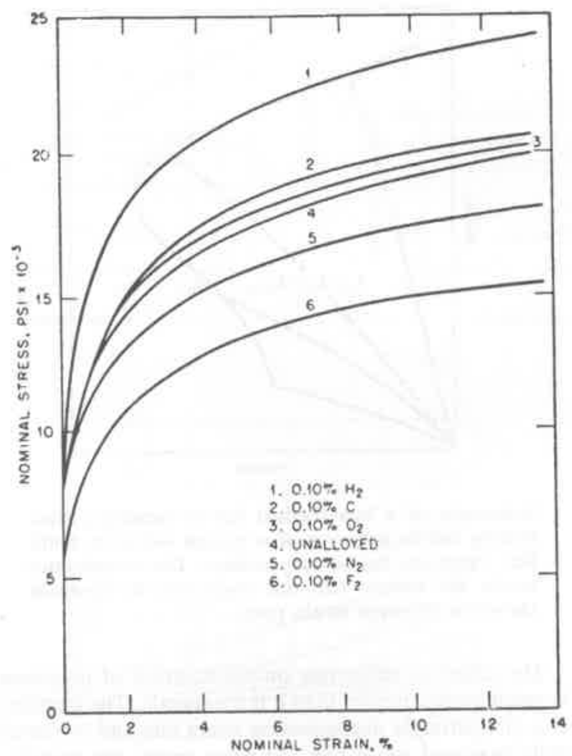

Portion of stress-strain relationships of alloys of annealed yttrium with H_2, C, O_2, N_2, and F_2.

Source: The Rare Earths, F. H. Spedding and A. H. Daane, Eds., John Wiley & Sons, Inc., London, 1961, p 447